# ESTIMATION OF SPATIO-TEMPORAL VARIABILITY OF ACTUAL EVAPOTRANSPIRATION USING THE SEBS MODEL IN THE SEMIARID BAROTSE BASIN, SOUTH-WESTERN ZAMBIA

W. K. Phiri[a,*], I. A. Nyambe[a], J. Kabika[a], Z. Vekerdy[b], T. Woldai[b]

[a] University of Zambia, IWRM Centre, C/O School of Mines, P.O. Box 32379, Lusaka, Zambia
[b]Faculty of Geo-Information Science and Earth Observation (ITC), University of Twente, The Netherlands
[*]Corresponding author e-mail: wilsonphirik@yahoo.com

## ABSTRACT

*Evapotranspiration (ET) is a dominant hydrologic loss flux in the water budget of arid and semi-arid areas. Thus, accurate estimation of its dynamics is critical for assessing water availability and improving water resources management in such areas. In this study the physically-based Surface Energy Balance System (SEBS) model was applied to estimate spatio-temporal variability of actual ET (AET) in the semiarid Barotse basin, South-Western Zambia. The model was run using atmospherically rectified MODIS satellite imagery on clear-sky warm-wet, cool-dry and hot-dry days. Furthermore, based on sunshine hours and daily AET, monthly fluxes were generated. The outputs were evaluated against potential ET (PET) and independently modelled AET from the global circulation model of the European Centre for Medium-range Weather Forecast (ECMWF). It was observed that the ratio of AET to PET at the reference station was in the order of 1.04, 0.64 and 0.30 on warm-wet, cool-dry and hot-dry days respectively. Systematic lack of physical agreement on warm-wet days suggested that SEBS estimates were not necessarily implausible but that assumptions on which PET is based differed from surface conditions. ECMWF estimates were in better agreement with SEBS at daily and monthly time-steps at Sesheke station than at Kamanga. This was ascribed to input data and vegetation index-based roughness parametrisation. Sensitivity analysis of the model to landuse-based versus NDVI aerodynamic roughness revealed a reduction of fluxes of up to 1.5 mm day$^{-1}$ on forests using the latter. Flux analysis showed that water bodies and regularly flooded vegetation had the highest rates of 6.9 and 5.9 mm day$^{-1}$ on warm-wet days respectively. The lowest occurred on croplands and grasslands with a high variation between warm-wet and hot-dry days of up to 64.1 and 71.1% respectively. It is concluded that SEBS model can accurately estimate AET in heterogeneous areas with spatial input data and robustly determined roughness values.*

***Keywords:*** *Actual evapotranspiration, spatio-temporal variability, aerodynamic roughness, SEBS, MODIS*

## INTRODUCTION

Evapotranspiration (ET) is a key component in the water budget of arid and semi-arid areas, as it is a dominant hydrologic loss flux (Khan, *et al*., 2010). The ratio of ET to precipitation over these climatic regimes nears 100 percent under dry conditions (Irmark, 2009). Thus, accurate estimation of its spatio-temporal dynamics in such areas is critical for assessing surface and groundwater availability (Huxman, 2005), improving agriculture water resources management (Rwasoka, *et al*., 2011), determining water use of vulnerable ecosystems and predicting climate variability and change (van der Kwast, *et al*., 2009). However, there is a caveat in correctly representing distributed ET over heterogeneous areas. This stems from the

complex relationship among numerous elements in the land-plant-atmosphere system that influences ET, namely; surface characteristics (e.g roughness, albedo, vegetation height, and rooting depth), soil properties (e.g retention and conductivity) and meteorological conditions (e.g solar radiation, air pressure, temperature and humidity). Consequently, the common method of estimating ET assumes a homogenous surface for calculation of potential ET (PET) or a reference ET ($ET_o$) at points, rather than spatio-temporal actual ET (AET). A plethora of formulae used to estimate PET exist and include the Penman (Penman, 1948), Priestley and Taylor (Priestley and Taylor, 1972) and FAO-Penman-Montieth (Allen et al., 1998) equations. On the other hand, direct measurement of turbulent heat fluxes is widely done using Bowen ratio and eddy co-variance methods at field scale. Similar techniques are used in ambitious programmes to estimate heat fluxes over several square kilometres using instruments onboard aircrafts. For practical purposes, all these methods should be valid over small areas. However, effective water resources management entails understanding fluxes at a meaningful hydrologic unit such as a catchment, which often occur at a large scale. This is especially important in water-short areas where inaccurate data can lead to large errors in the prediction of water resources availability. Thus, the use of methods that capture distributed fluxes at a large scale will go a long way in meeting such objectives.

Fortunately, in the recent past remote sensing has become a pragmatic approach for estimating distributed ET, especially with the availability of large amounts of satellite data. This has presented unprecedented opportunities for understanding the dynamics of surface-atmospheric interactions. A host of remote sensing techniques of varying complexity have been proposed for the estimation of ET since the pioneering works of Jackson (1977) and, Seguin and Ittier (1983) by various researchers. In the present study, the physically-based Surface Energy Balance System (SEBS) model proposed by Su (2002) in combination with meteorological data was applied over the semiarid Barotse basin, South-Western Zambia and the objectives were to: 1) estimate AET over different land cover on typical clear-sky warm-wet, cool-dry and hot-dry days; 2) generate monthly evaporative fluxes from daily AET and sunshine hours; 3) determine daily PET using the FAO Penman-Montieth method; and 4) evaluate the SEBS modelled evaporative fluxes against calculated PET and independently modelled AET from the Global Circulation Model (GCM) of European Centre for Medium-range Weather Forecast (ECMWF). In this study, the SEBS model was run using atmospherically rectified Moderate-resolution Imaging Spectoradiometer (MODIS) satellite imagery on clear sky warm-wet, dry-cool and dry-hot days. Specifically, evaporative fluxes were estimated over eight different land cover types. The modelled evaporative fluxes at daily and monthly time step were evaluated against PET and AET from ECMWF at Sesheke and Kamanga reference stations.

Motivation to undertake this study came from a number of concerns. The semiarid Barotse basin lies in the agro-ecological regime of Zambia that frequently receives below normal rainfall and experiences critical water shortages in the dry season. It is also a subject of study for the projected effects of climate variability and change (Flint, 1999). The amount of soil moisture available to the root crop, fresh water available for aquifer recharge and human uses in this area is highly influenced by the narrow difference between precipitation and ET. Presently, groundwater is the major source of fresh water for domestic use but the recharge rates, which are affected by high rate of ET, are unknown. Furthermore, due to dilapidated monitoring infrastructure, ET in this basin is estimated from limited

meteorological stations. Although use of remote sensing can fill this vacuum, fewer studies have been carried out, especially with respect to use of the SEBS model in southern Africa (Rwasoka et al., 2011). Yet many of the countries in the region need to cooperate in the management of shared waters following the water sector reforms in which water resources management are to be initiated at catchment and basin scales. Thus, the use of remote sensing data in water-short areas of this region, especially in those parts with limited meteorological stations, will be critical to informed planning, monitoring and management of water resources.

## DESCRIPTION OF THE STUDY AREA

The semiarid Barotse basin is located in the Southwest of Zambia (Figure 1). It lies between Longitudes 23° and 27° East and Latitudes 15° and 18° South. It sits on an average elevation of 900 metres a.s.l and occupies an area of 45,568Km$^2$. It experiences a tropical savanna climate with three distinct seasons: warm-wet (November to March), cool-dry season (April to July) and dry-hot-season (August to October). The annual rainfall is 657 mm around Sesheke District, one of the lowest in Zambia. Pan evaporation is at 1860 mm. Mean temperatures rise as high as 34.2° C (October) and drops to 4.4°C (July).

## MATERIALS AND METHODS

### The concept of the Surface Energy Balance System model

The SEBS model was formulated for the determination of turbulent heat fluxes using spectral reflectance and radiance data from satellite observations together with meteorological data. In this paper the salient concept of the model are presented. A full description of its theoretical basis is given in Su (2002; 2005) and Su et al. (2003). In principle, the SEBS is a one-source physical model (van der Kwast, 2009) which estimates turbulent heat fluxes based on the energy balance equation given in Eq. (1).

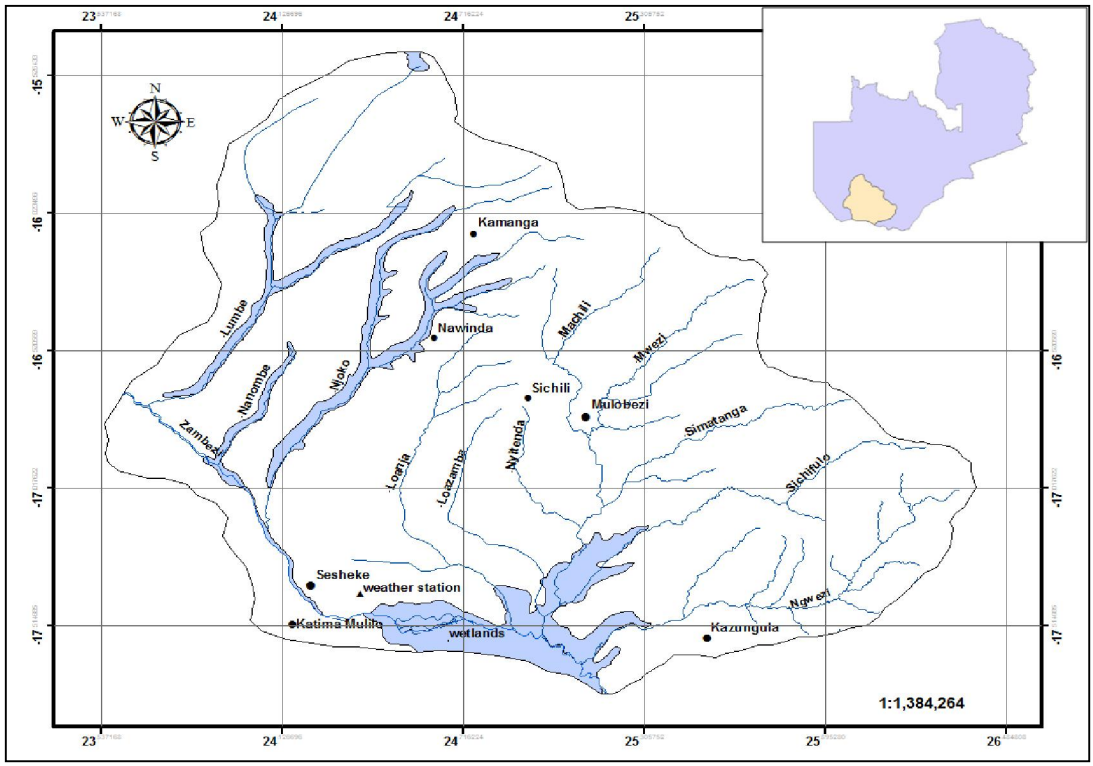

Figure 1: Location of study area of the semi-arid Barotse basin, Southwest Zambia

$$R_n = G + H + \lambda ET \quad (1)$$

where $R_n$ is net radiation ($Wm^{-2}$), H is sensible heat ($Wm^{-2}$), G is soil heat flux ($Wm^{-2}$), $\lambda ET$ is latent heat flux ($Wm^{-2}$). Net radiation, which is the sum of total incoming shortwave radiation and outgoing long wave radiation at the Earth's surface, is estimated in the SEBS as expressed in Eq. (2).

$$R_n = (1 - \alpha).R_{swd} + \varepsilon.R_{lwd} - \varepsilon.\sigma.T_0^4 \quad (2)$$

where $\alpha$ is albedo, $R_{swd}$ is shortwave downward radiation ($Wm^{-2}$), $R_{lwd}$ is downward longwave radiation ($Wm^{-2}$), $\varepsilon$ is emissivity, $\sigma$ is the Stephan-Boltzman constant ($Wm^{-2}\ K^{-4}$), $T_0$ is surface temperature (K)

The soil heat flux, the energy that is conducted into the soil, was calculated as a fraction of net radiation following the method proposed by Choudhury et al. (1994) given in Eq. (3).

$$G_o = R_n[\Gamma_c + (1 - f_c)(\Gamma_s - \Gamma_c)] \quad (3)$$

where, $\Gamma_c$ and $\Gamma_s$ are soil heat flux ratios for a full vegetation canopy which is 0.05 (Monteith and Unsworth, 1990) and bare soil taken as 0.315 (Kustas and Daughtry, 1990) and $f_c$ is vegetation fraction. Thus interpolation was performed between these limiting cases using the $f_c$ which was calculated from the empirical relationship with NDVI (Sobrino et al., 2003) as given in Eq. (4).

$$f_c = \frac{(NDVI - NDVI_{min})^2}{(NDVI_{max} - NDVI_{min})^2} \quad (4)$$

where $NDVI_{max}$ is taken be 0.5 and $NDVI_{min}$ taken as 0.2. These values were adopted as the scene or season dependent ones for the study were not yet known.

In the SEBS, the sensible heat is estimated from the combination of Eqs. (5), (6) and (7) based on the similarity theory as proposed by Monin and Obukhov (1954).

$$u = \frac{u_*}{k}\left[In\left(\frac{z - d_o}{z_{om}}\right) - \Psi_m\left(\frac{z - d_o}{L}\right) + \Psi_m\left(\frac{z_{om}}{L}\right)\right] \quad (5)$$

$$\theta_o - \theta_a = \frac{H}{ku_*\rho C_p}\left[In\left(\frac{z - d_o}{z_{oh}}\right) - \Psi_h\left(\frac{z - d_o}{L}\right) + \Psi_h\left(\frac{z_{oh}}{L}\right)\right] \quad (6)$$

$$L = \frac{\rho C_p u_*^3 \theta_v}{kgH} \quad (7)$$

where z is reference height (m), $u_*$ is friction velocity, $\rho$ is density of air, k is von Karman's constant, $d_o$ is zero displacement height (m), $z_{om}$ is roughness height for momentum transfer (m), $Z_{oh}$ is roughness length for heat transport, $\rho$ is density of air, $C_p$ Specific heat capacity of dry air, $\theta_o$ and $\theta_a$ are potential temperature at surface and air (K), $\Psi_m$ and $\Psi_h$ are stability correction functions for momentum and sensible heat transfer respectively, L is Obukhov length, g is acceleration due to gravity and $\theta_v$ is potential virtual temperature (K). In the SEBS, sensible heat is constrained by the wet limit ($H_{wet}$) and dry limit ($H_{dry}$). At the dry limit, ET approaches zero due to the limitation of soil moisture and sensible heat ($H_{dry}$) takes its maximum value. This relationship is expressed as given in Eq. (8) (Su, 2002).

$$\lambda E_{dry} = R_n - G_0 - H_{dry} \equiv 0 \quad or \quad H_{dry} = R_n - G_o \quad (8)$$

At the wet limit, sensible heat is at its minimum value and evaporation takes place at the potential rate and is limited only by energy at surface. The relationship is defined as given in Eq. (9) (Su, 2002).

$$\lambda E_{wet} = R_n - G_o - H_{wet} \quad or \quad H_{wet} = R_n - G_0 - \lambda E_{wet} \quad (9)$$

According to Su (2002), the equation similar to the FAO Penman-Montieth (Allen, *et al.*, 1998) is combined with equation (9) to

calculate sensible heat at the wet limit as given in Eq. (10).

$$H_{wet} = \left((R_n - G_o) - \frac{\rho c_p}{r_{ew}} . \frac{e_s - e_a}{\lambda}\right) / \left(1 + \frac{\Delta}{\lambda}\right) \quad (10)$$

where $e_a$ is actual vapour pressure (Pa), $e_s$ is saturation vapour pressure (Pa), $\gamma$ is psychrometric constant (kPa $^oC^{-1}$), $\Delta$ is rate of change of saturation vapour pressure with temperature (kPa $^oC^{-1}$) and $r_{ew}$ is external resistance. The evaporative fraction is determined as given in Eq. (11) (Su, 2002).

$$\Lambda = \frac{\lambda E}{R_n - G} \quad (11)$$

Finally, daily AET is calculated by assuming the evaporative fraction is constant the whole day (Jia, *et al*., 2009). The instantaneous values were upscaled to daily ET as given in Eq. (12).

$$AET_{daily} = 8.64 \times 10^7 \times \left[\Lambda . \frac{R_{ndaily} - G_{daily}}{\lambda \rho_w}\right] \quad (12)$$

where, $\rho_w$ is density of water (kg $m^3$) and $R_{ndaily}$ is daily net radiation ($Wm^2$), $G_{daily}$ is daily soil surface heat flux ($Wm^2$), $\lambda$ is latent heat of vapourisation ($Jkg^{-1}$). In this study, the estimates of monthly evaporative fluxes were also required. To achieve this, a method proposed by Gokmen et al. (2012) that mimics energy and soil moisture constraints in the ET process was used and is given in Eq. (13).

$$ET_{n\ daily} = ET_{daily}\left(\frac{sunhours_{n\ daily}}{sunhours_{\ daily}}\right) \quad (13)$$

where, $ET_{n\ daily}$ is ET for n cloud free day, $sunhours_{n\ daily}$ is cumulative sum of sunshine hours for n days, $sunhours_{\ daily}$ is the sunshine duration for a cloud free day (Gokmen, *et al*., 2012).

**Satellite image acquisition and pre-processing**

In this study, Level 1B calibrated MODIS radiance and reflectance images were used. These images were carefully selected to represent typical warm-wet, cool-dry and hot-dry clear-sky days (Table 1).

Table 1: MODIS satellite images used in the study

| No. | Year | Day of Year (DOY) | Overpass Time (GMT) | No. | Year | Day of Year (DOY) | Overpass Time (GMT) |
|---|---|---|---|---|---|---|---|
| 1. | 2006 | 325 | 08:25 | 13. | 2007 | 136 | 08:45 |
| 2. | 2006 | 334 | 08:40 | 14. | 2007 | 143 | 08:50 |
| 3. | 2006 | 336 | 08:25 | 15. | 2007 | 168 | 08:45 |
| 4. | 2006 | 338 | 08:15 | 16. | 2007 | 170 | 08:35 |
| 5. | 2007 | 12 | 08:20 | 17. | 2007 | 191 | 08:50 |
| 6. | 2007 | 14 | 08:10 | 18. | 2007 | 197 | 08:15 |
| 7. | 2007 | 45 | 09:05 | 19. | 2007 | 225 | 08:40 |
| 8. | 2007 | 49 | 08:40 | 20. | 2007 | 232 | 08:45 |
| 9. | 2007 | 71 | 08:05 | 21. | 2007 | 255 | 08:50 |
| 10. | 2007 | 74 | 08:35 | 22. | 2007 | 257 | 08:46 |
| 11. | 2007 | 106 | 08:35 | 23. | 2007 | 287 | 08:50 |
| 12. | 2007 | 113 | 08:40 | 24. | 2007 | 292 | 09:10 |

The images were downloaded from NASA`s Level 1 and Atmosphere Achieve and Distribution System (LAADS) website (http://ladsweb.nascom.nasa.gov/). The chosen images were re-projected from their native format (sinusoidal) to geographic format and resampled to a uniform resolution of 1km using MODIS Re-projection Swath Tool (MRTSwathTool). The parameters used were: resample method - nearest neighbour; output projection type - Geographic; output file type - Geotiff; and output resolution was 1km. The specific channels utilised were the reflective visible and near-infrared range (bands 1-7) and thermal emission range (bands 31 and 32), together with geo-location files. The Geotiff files were imported into Integrated Land and Water information Software (ILWIS) for processing and computing the surface energy balance.

**Atmospheric correction of the visible bands**

The correction of satellite images for the effects of atmospheric absorption and attenuation is important for any approach concerned with the energy balance equation. In this study, for the effects of scattering and absorption in the visible and near-infrared bands was done using the Simplified Method for Atmospheric Correction (SMAC) algorithm by Rahman and Dedieu (1994). The input data were: optical thickness (AOT) at 0.55µm, ozone concentration, water vapour content, surface pressure, satellite and solar view angles, and coefficient files. AOT was estimated from visibility measurements following the procedure of MacClatchey and Selby (1972). The required water vapour data was obtained from the AERONET website (http://aeronet.gsfc.nasa.gov/) whereas ozone data was retrieved from the OMI Ozone monitoring project website (http://toms.gsfc.nasa.gov/ozone/ozone_v8.html).

**Parametrisation of biogeophysical parameters**

The required biogeophysical parameters were calculated from remote sensing data following established methods, namely; albedo by Liang (2001), surface emissivity, fractional vegetation cover, leaf area index (LAI) and land surface temperature by Sobrino, *et al*. (2003), and Normalised Difference Vegetation Index (NDVI) as first described by Tucker (1979). From the vegetation indices, roughness height for momentum transfer ($Z_{om}$) and roughness height for heat transfer ($z_{oh}$) were calculated as proposed by Su (2002). Displacement height ($d_o$) and vegetation height were estimated using the formula by Brutsaert (1982). In addition, a $Z_{om}$ map based on landuse type was constructed using literature values found in Wieringa (1993), Mücher et al. (2001) and Su (2005) and used to run the SEBS model. This was done as $Z_{om}$ values estimated from NDVI tend to be very low over tall elements (Su, 2005).

**Meteorological data**

Meteorological inputs required to run the SEBS model were: solar radiation, air temperature, specific humidity, wind speed and pressure at the surface and reference height. Few variables were available at the reference station over satellite passing time. The gap was solved by: (1) using empirical formulae (2) retrieving such data from GCMs. Thus, atmospheric variables which are related to temperature were calculated using formulae as described in Allen et al. (1998) whereas solar radiation and surface pressure were obtained from the ECMWF website (http://www.ecmwf.int/).

**Land cover**

The land cover map used in this study was derived from the European Space Agency (ESA) Globcover Project of 2008. It is a Medium Resolution Imaging Spectrometer (MERIS) digital map of a spatial resolution of 300m (Bicheron et al., 2008) which is

accessible on http://www.esa.int/due/ionia/globcover together with the validation report free of charge. The extracted land cover map of the study area was validated against ground truth data that was collected during the field work campaign. Fifty-three field-points were collected in this campaign. Furthermore, sixty-five sample points were randomly selected over the study area for quality assessment. The true ground cover (reference data) for these points was obtained from a visual interpretation of very high resolution Google Earth images. The land cover map of the semiarid Barotse basin and some validation points are shown in Figure 2.

The analysis of consumptive water use in this study was based on eight land cover types: mosaic vegetation/Croplands (30), closed broadleaved deciduous forest (50), open broadleaved deciduous forest (60), mosaic grassland/forest-shrubland (120), closed to open shrubland (130) closed to open grassland (140), closed to open vegetation regularly flooded (180) and water bodies (210). The distribution of land cover types by percentage in the semiarid Barotse basin is shown in Table 2.

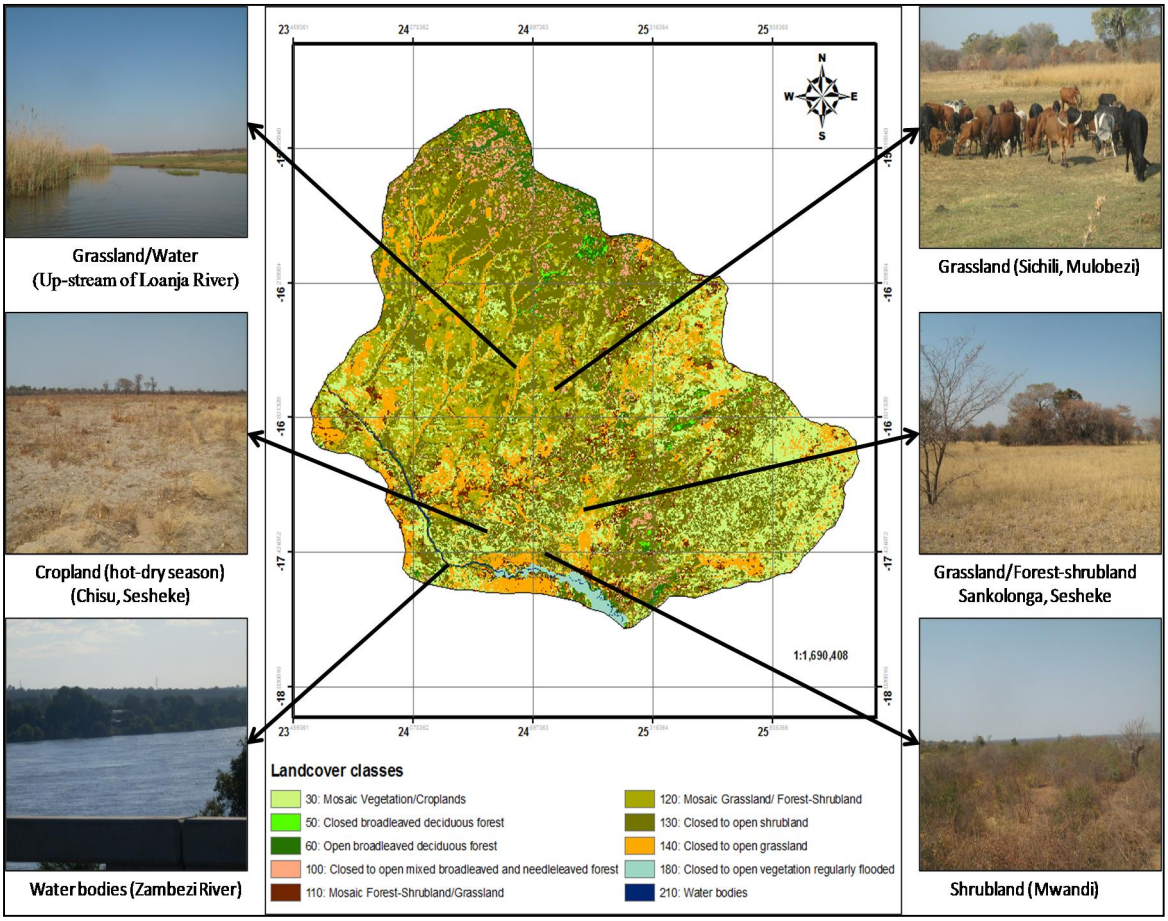

Figure 2: Land cover types in the semi-arid Barotse basin (modified after Bicheron et al., 2008)

Table 2: Land cover type by percentage in the semiarid Barotse Basin (adapted from Bicheron, *et al*., 2008)

| Land cover code | Land cover type | Percentage of the area |
|---|---|---|
| 30 | Mosaic vegetation/Cropland | 20.78 |
| 50 | Closed broadleaved deciduous forest | 0.37 |
| 60 | Open broadleaved deciduous forest | 2.98 |
| 100 | Closed to open mixed broadleaved and needleleaved forest | 2.77 |
| 110 | Mosaic forest shrubland/Grassland | 3.93 |
| 120 | Mosaic grassland/Forest shrubland | 18.57 |
| 130 | Closed to open shrubland | 34.79 |
| 140 | Closed to open grassland | 14.56 |
| 180 | Closed to open vegetation regularly flooded | 0.77 |
| 210 | Water bodies | 0.48 |

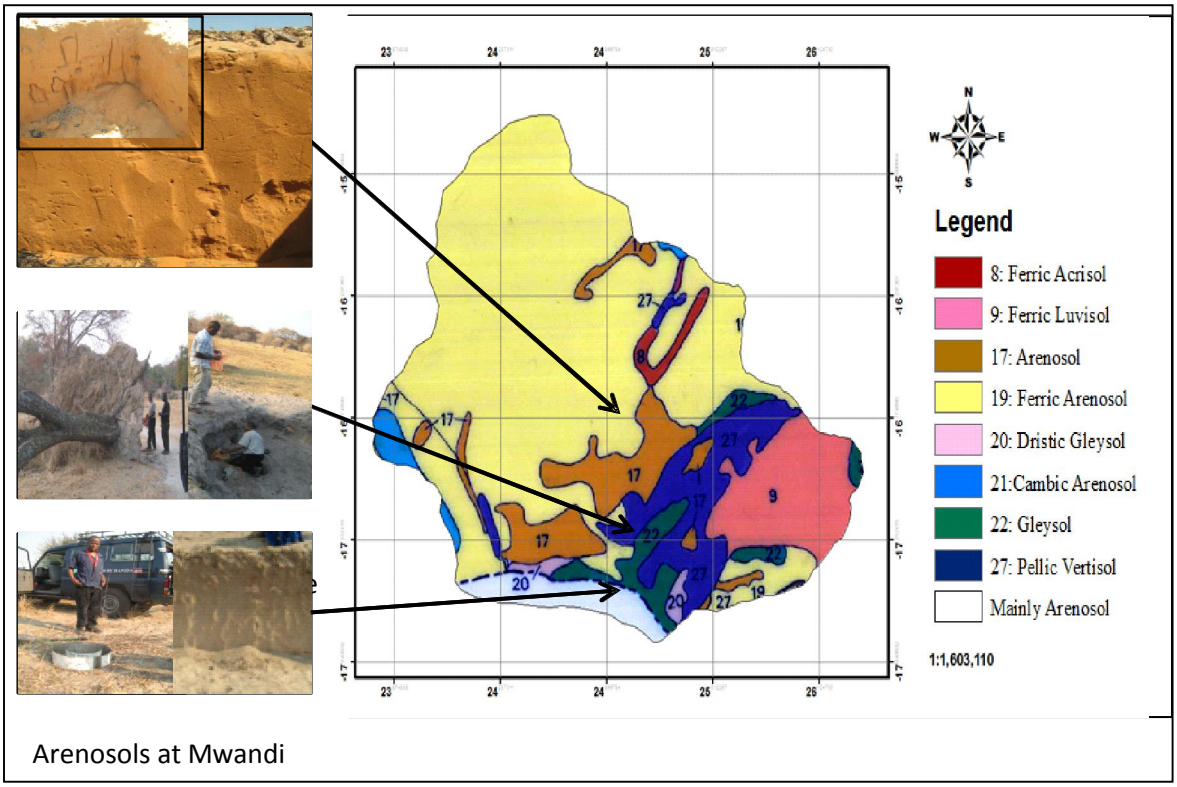


Figure 3: Soil types in the semiarid Barotse basin, South-Western Zambia (modified from FAO and GRZ, 1986)

**Soil type**

The soil and sample types that were physically examined in the field over the study area are shown in Figure 3. The predominant are arenosols. These are marked by a sandy texture, lack of significant profile development, excessive permeability and low nutrient content. For these reasons, farming on this soil type is limited. The vertisols have a high content of expansive clay that forms deep cracks in the dry season, and a high water holding capacity because of a heavy clayey proportion. The natural vegetation on this soil is grass woodland as the heavy texture

and unstable behaviour of the soil cannot support tree species. Gleysol is typically confined to the wetlands areas. Grass is a dormant vegetation cover on this soil. Luvisol is characterised by some nutrient content and better drainage. Thus farming is confined on this soil type apart from Gleysol and vertisols (FAO and GRZ, 1986).

## RESULTS AND DISCUSSION

### Accuracy assessment of the land cover map used

The accuracy of the land cover map of the study area was assessed using ground data. The results are shown in the contingency matrix in Table 2. The main diagonal shows the number of correct points. An overall accuracy of 79.9% and kappa statistic of 74.4% were obtained. It was observed that errors were relatively higher on 'mixed' land cover. For instance, omission and commission errors on closed to open grassland (140) were at 21.1% and 31.8% respectively. This was ascribed to fuzziness. A fussy land cover has a large spectral variability, which usually contributes to misclassification (Bicheron et al., 2008).

Table 2: Error matrix of the ESA Globcover-2008 land cover product over the Barotse Sub-basin

| ESA-2008 classification code | Reference (field data and visually interpreted points from very high resolution Google Earth imagery) | | | | | | | | Total No. | User`s accuracy (%) |
|---|---|---|---|---|---|---|---|---|---|---|
| | 30 | 50 | 60 | 120 | 130 | 140 | 180 | 210 | | |
| 30 | 17 | 0 | 0 | 0 | 2 | 2 | 0 | 0 | 21 | 81.0 |
| 50 | 0 | 7 | 1 | 0 | 0 | 0 | 0 | 0 | 8 | 87.5 |
| 60 | 0 | 1 | 11 | 0 | 2 | 0 | 0 | 0 | 12 | 91.7 |
| 120 | 2 | 0 | 0 | 10 | 0 | 0 | 0 | 0 | 14 | 71.4 |
| 130 | 2 | 0 | 1 | 2 | 14 | 1 | 0 | 0 | 20 | 70.0 |
| 140 | 2 | 0 | 0 | 2 | 0 | 15 | 1 | 2 | 22 | 68.2 |
| 180 | 0 | 0 | 0 | 0 | 0 | 1 | 9 | 1 | 11 | 81.8 |
| 210 | 0 | 0 | 0 | 0 | 0 | 0 | 1 | 9 | 10 | 90.0 |
| Total No. | 23 | 8 | 13 | 14 | 18 | 19 | 11 | 12 | 118 | Accuracy: 79.9% Kappa statistic: 74.4% |
| Producer`s accuracy | 73.9 | 87.5 | 84.6 | 71.4 | 77.8 | 78.9 | 81.8 | 75.0 | | |

### The estimated SEBS fluxes by land cover type on warm-wet days

The average estimates of AET and biogeophysical parameters per land cover type on warm-wet days are shown in Table 3. Water bodies (210) and closed to open regularly flooded vegetation (180) had higher ET rates of ~6.9 and 5.9 mm day$^{-1}$ respectively. This was ascribed to availability of 'moisture' and the influence of lower albedo, which controls the amount of energy available at the surface. On the other hand, high rates of ET over closed broadleaved deciduous forest (50), open broadleaved deciduous forest (60) and other forested areas were associated with high photosynthetic activity and moisture evidenced by high NDVI values. Lower fluxes occurred on mosaic vegetation/croplands (30) and closed to open grassland (140) due to the combined effect of higher albedo and lower NDVI values (cf. Alvarez, 2007).

Table 3: Average SEBS estimates of fluxes by land cover on warm-wet days in the semi-arid Barotse basin

| Land cover type (code) | Surface Albedo (-) | NDVI (-) | $Z_{om}$ (m) | Net Radiation ($Wm^{-2}$) | Surface Temperature (K) | Average AET ($mmday^{-1}$) |
|---|---|---|---|---|---|---|
| 30 | 0.14 | 0.54 | 0.08 | 643 | 298 | 3.6 |
| 50 | 0.13 | 0.71 | 0.06 | 699 | 296 | 5.8 |
| 60 | 0.11 | 0.74 | 0.07 | 700 | 297 | 5.4 |
| 120 | 0.12 | 0.70 | 0.08 | 640 | 303 | 5.0 |
| 130 | 0.12 | 0.67 | 0.10 | 659 | 304 | 5.3 |
| 140 | 0.13 | 0.52 | 0.08 | 614 | 305 | 4.6 |
| 180 | 0.10 | 0.37 | 0.07 | 651 | 301 | 5.9 |
| 210 | 0.08 | 0.15 | 0.01 | 706 | 297 | 6.9 |

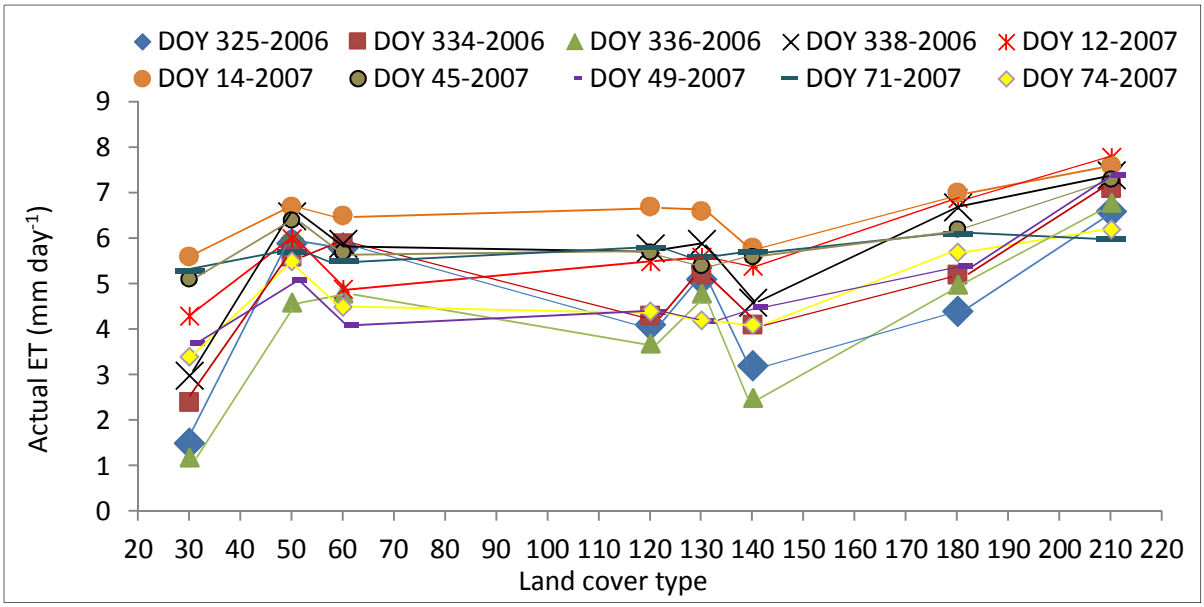


Figure 4: Variation of mean AET by land cover type on warm-wet days in the semi-arid Barotse basin

The flux trends on warm-wet days (Figure 4) depict 'peaks' on forested areas and water bodies (210), and 'troughs' over grasslands (140) and croplands (30). The maximum mean rate on water bodies and regularly flooded vegetation was 7.8 and 7.0 mm $day^{-1}$ respectively. High ET over forests is shown by the peaks at broadleaved deciduous forest (50) broadleaved deciduous forest (60), mosaic grassland/forest-shrubland (120) and closed to open shrubland (130). It is observed that ET increased between DOY 325 (21st November) to DOY 14 (14th January), and the highest rates occurred on DOY 12 and 14. Historically, ~90 % of rainfall in the area falls between November and March. Thus, higher ET appeared to occur contemporaneously with the increase in the occurrence of rainfall events in the study area.

**The estimated fluxes per land cover type on cool-dry days**

The average AET and biogeophysical parameters per land cover type on cool-dry days are shown in Table 4. Water bodies (210) and closed broadleaved deciduous forest (50) had higher evaporative rates of ~5.0 and 4.8 mm $day^{-1}$ respectively. The

fluxes on open broadleaved deciduous forest (60), mosaic grassland/forest-shrubland (120) and closed to open regularly flooded vegetation (180) ranged from 4.0 to 4.4 mm day$^{-1}$. Lower rates occurred on grasslands (140) and mosaic vegetation/croplands (30).

The mean AET per land cover type on cool-dry days is shown in Figure 5. Evaporative water use of mosaic grassland/forest-shrubland (120) and closed to open shrubland (130) varied from 1.2 to 5.9 mm day$^{-1}$. The mean fluxes over closed to open grassland (140) and mosaic vegetation/croplands (30) ranged from 0.3 to 4.6 mm day$^{-1}$. On the other hand, ET over water bodies (210) and closed broadleaved deciduous forest (50) was higher. It ranged from 4.0 to 6.8 mm day$^{-1}$. High flux rates were also observed over open broadleaved deciduous forest (60) and closed to open regularly flooded vegetation (180).

Table 4: Average estimates of SEBS fluxes by land cover on cool-dry days in the semi-arid Barotse basin

| Landcover type (code) | Surface Albedo* (-) | NDVI* (-) | $Z_{om}$* (m) | Net Radiation (Wm$^{-2}$) | Surface Temperature (K) | Daily AET (mmday$^{-1}$) |
|---|---|---|---|---|---|---|
| 30 | 0.08 | 0.64 | 0.06 | 436 | 297 | 1.8 |
| 50 | 0.05 | 0.90 | 0.04 | 477 | 294 | 4.8 |
| 60 | 0.04 | 0.87 | 0.05 | 478 | 295 | 4.4 |
| 120 | 0.07 | 0.73 | 0.07 | 439 | 300 | 4.0 |
| 130 | 0.07 | 0.77 | 0.05 | 443 | 298 | 3.1 |
| 140 | 0.09 | 0.59 | 0.07 | 426 | 298 | 2.1 |
| 180 | 0.05 | 0.86 | 0.04 | 472 | 295 | 4.4 |
| 210 | 0.02 | 0.00 | 0.00 | 475 | 293 | 5.0 |

Asterisk* means the average exclude values for days in July

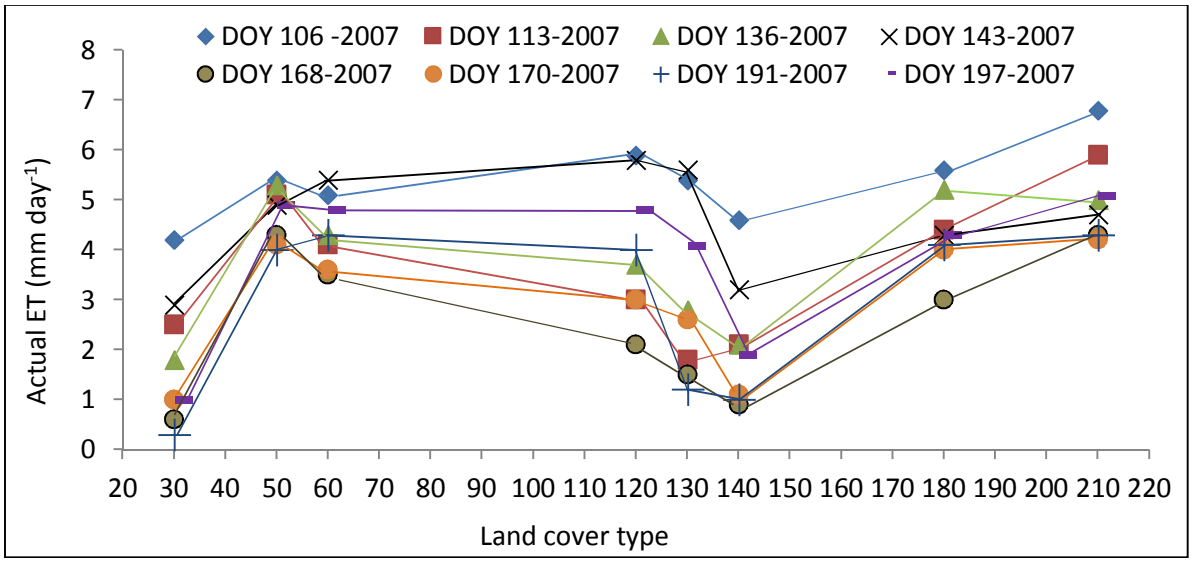


Figure 5: Variation of mean AET by land cover type on cool-dry days in the semi-arid Barotse basin

**The estimated SBES fluxes per land cover type on hot-dry days**

The average ET and surface parameters on hot-dry days are shown in Table 5. The rate of ET over mosaic vegetation/croplands (30) and grasslands (140) was very low due drier conditions as evidenced by lower NDVI and higher surface temperatures. On the other hand, the rates were higher over water bodies (210) and closed to open regularly flooded vegetation (180) due to the availability of moisture. The fluxes over forested areas such as broadleaved deciduous forest (50) and open broadleaved deciduous forest (60) ranged from moderate to high. Over these surfaces, ET tended to be high with NDVI and at variance with surface temperature (cf. Jackson et al., 1977; Moran et al., 1994; Carlson et al., 1995).

The scatter of evaporative fluxes on hot-dry days per land cover type is shown in Figure 6. Grasslands (140) and mosaic vegetation/croplands (30) had lower mean values of ET which ranged from 0.8 to 2.2 mmday$^{-1}$. On the other hand, higher mean values of 7.7 and 5.6 mm day$^{-1}$ were observed over water bodies (210) and open regularly flooded vegetation (180) respectively. The flux rates over closed broadleaved deciduous forest (50), open broadleaved deciduous forest (60), mosaic grassland/ forest-shrubland (120) and closed to open shrubland (130) varied in the region of 2.4 to 4.7 mm day$^{-1}$.

Table 5: Average estimates SEBS fluxes by land cover on hot-dry days in the semi-arid Barotse basin

| Land cover Type (code) | Surface Albedo (-) | NDVI (-) | $Z_{om}$ (m) | Net Radiation (Wm$^{-2}$) | Surface Temperature (K) | Daily AET (mmday$^{-1}$) |
|---|---|---|---|---|---|---|
| 30 | 0.12 | 0.35 | 0.09 | 465 | 308 | 1.1 |
| 50 | 0.08 | 0.73 | 0.06 | 524 | 301 | 3.9 |
| 60 | 0.07 | 0.70 | 0.06 | 551 | 300 | 3.6 |
| 120 | 0.13 | 0.48 | 0.09 | 458 | 310 | 3.5 |
| 130 | 0.11 | 0.56 | 0.08 | 454 | 309 | 3.0 |
| 140 | 0.11 | 0.41 | 0.09 | 455 | 310 | 1.3 |
| 180 | 0.09 | 0.66 | 0.07 | 493 | 305 | 4.6 |
| 210 | 0.04 | 0.12 | 0.00 | 550 | 300 | 6.7 |

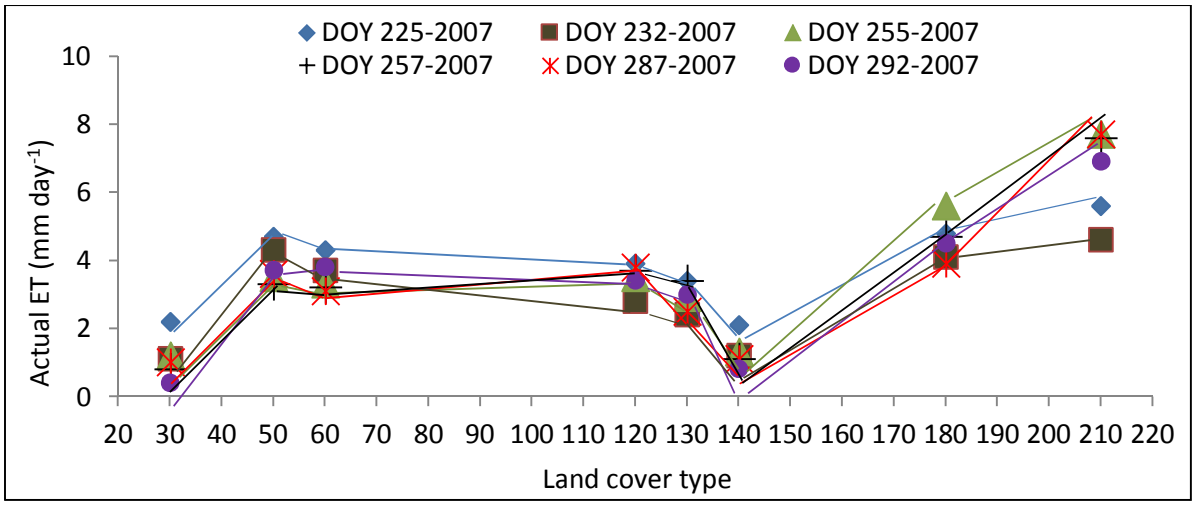


Figure 6: Variation of mean AET by land type on hot-dry days in the semiarid Barotse basin

The spatio-temporal variability of AET is depicted by representative days (Figures 7-9). The fluxes on warm-wet day are shown on DOY 12 at the height of the rain season (Figure 7). Due to increased moisture, ET was very high on this day. On the other hand, Figure 8 depicts AET on a cool-dry on DOY 170. The values here were lower due to declining soil water and reduced energy as it is in the cold season. The effect of declining moisture is inferred from changes in the ET over croplands, which are located in the south-western part of the study area. These areas were expected to have lower rates of ET as the rain-fed crops would have been harvested by this time. The dominant process on such areas is expected to be evaporation than transpiration (cf. Shan et al., 2007). If soil moisture is limited, however, ET occurs at a lower rate. This is why ET over these surfaces was lower than that over water bodies and forested areas.

The major sources of high fluxes on this day were confined to water bodies in the south and forested areas in the north. Relatively high energy associated with the hot season intensified ET over these surfaces. By contrast, the south-eastern parts experienced lower rates due to decreased soil water on croplands and grasslands, which by this time would be dry. Thus, the variation of AET was higher on these land cover types compared to water bodies and forested areas (Figure 10).

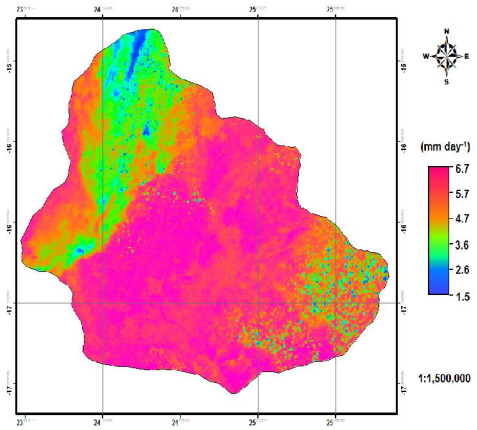


Figure 7: AET on DOY 12, semiarid Barotse basin

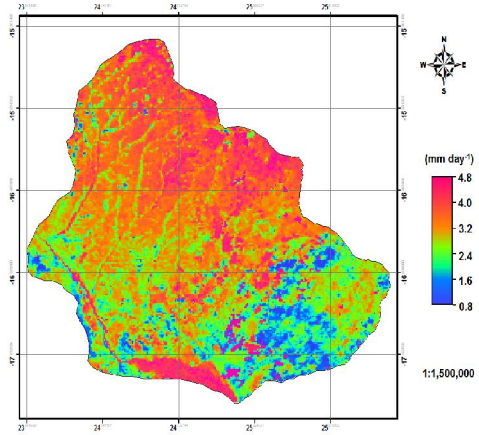


Figure 8: AET on DOY 170, semiarid Barotse basin

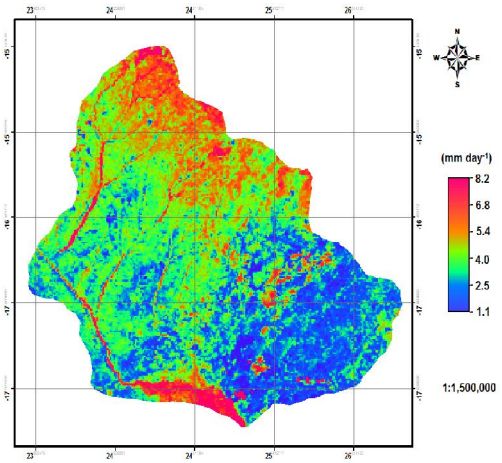


Figure 9: AET on DOY 257, semiarid Barotse basin

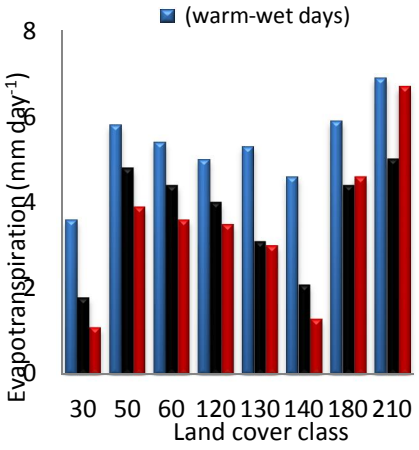


Figure 10: Variation of AET in the semiarid Barotse basin

**Estimated monthly evaporative fluxes from daily values and sunshine data**

The statistics of monthly evaporative fluxes are shown in Table 6. Due to the presence of water bodies, maximum evaporation rates were constantly high. These extreme values do not show the effects of soil moisture change but available energy. The decline in moisture on 'bare pixels'is inferred from minimum values. It was observed that mean fluxes ranged from 45 to 232 mm month$^{-1}$. The maximum rates varied from 129 to 356 mm month$^{-1}$ whereas the minimum ranged from Zero to 84.4 mm month$^{-1}$. The highest mean rates occurred in the wet-warm months (November to March). Over this period, the rate of ET was between 126 and 232 mm month$^{-1}$. In the cool-dry months (April to July), the fluxes ranged from 45 to 145 mm month$^{-1}$. The lowest rates occurred in the hot-dry months (August to October) and were between 56 and 78 mm month$^{-1}$. The spatial-temporal distribution of estimated monthly AET for the 2006/07 hydrological year is shown in Figure 11. It is observed that AET was on the increase from November to January over the basin. This was ascribed to increased soil water and blooming of many plant species, which is characteristic at the peak of the rain season.

On the other hand, distributed AET was on the decline from the month of March due to the reduction in rainfall events as this is usually the last month in which effective rainfall is received in the area. The reduction in the rate of ET in the month of June was attributed to the limitation of soil moisture and reduced energy at the surface.

As the hot-dry season approached in the month of August, the estimated AET was considerably lower especially in the south-eastern and south-western parts of the basin due to limitation of soil moisture. The amount of rainfall received over these areas is lower than that in the northern part (Hutchinson, 1974, MEWD-JICA, 1995). Furthermore, the intensification of heat in the hot dry season dried up the soils thereby reducing its moisture content further by the month of October. For this reason, ET was markedly high only over water bodies in the southern parts of the basin from August to October. High ET rates were also confined to forested areas in the northern parts of the basin during this period. This was because of the presence of relatively high moisture over these surfaces and the ability of tree species to draw water from deep surfaces using their long root system.

Table 6: Statistics of modelled monthly AET in the semiarid Barotse basin, South-Western Zambia

| (mm month$^{-1}$) | Nov | Dec | Jan | Feb | Mar | Apr |
|---|---|---|---|---|---|---|
| Minimum | 0.4 | 10.4 | 84.4 | 50.3 | 60.2 | 61.2 |
| Maximum | 276 | 275 | 304 | 231 | 272 | 242 |
| Mean | 137 | 145 | 232 | 155 | 126 | 145 |
| (mm month$^{-1}$) | May | Jun | Jul | Aug | Sept | Oct |
| Minimum | 2.6 | 0.0 | 0.0 | 0.0 | 0.0 | 0.0 |
| Maximum | 206 | 129 | 140 | 192 | 356 | 354 |
| Mean | 130 | 45 | 109 | 56 | 69 | 78 |

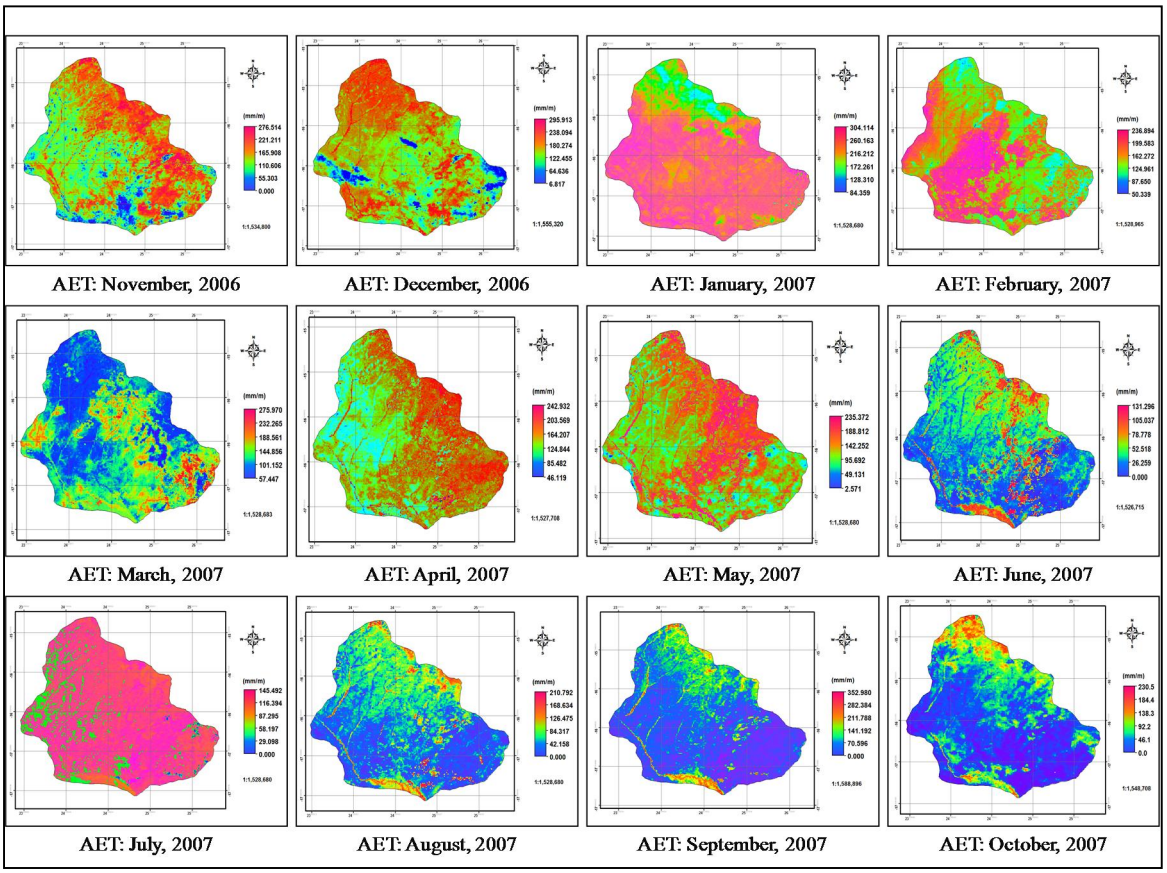


Figure 11: Estimated monthly AET in the semiarid Barotse basin for the 2006/07 hydrological year

The rest of the study area experienced lower rates of ET because of the loss of soil moisture via deep percolation and high rate of ET. This means the lower rates of ET over other vegetated surfaces indicated the adaptive mechanism which plant species employ to survive the dry conditions. Most of the plant species in the study area are deciduous (Jeans, 1991; Aregheore, 2006). These shade their leaves in the dry season to reduce transpiration. This explains why the evaporative fluxes were lower over plant species such as open shrublands and mosaic vegetation in the southern part of the study area in this dry month. The high rates of ET observed in isolated areas in the southern part of the basin were attributed to the wetter vertisols. These heavy clayey soils have a high retention capacity and remain relatively wet long after the rain season. These soils are characterised by high evaporative rates relative to other soils because of their high water holding capacity (cf. Suleiman and Richie, 2003).

### *4.6 Evaluation of modelled SEBS evaporative fluxes at a daily time scale*

The SEBS fluxes at Sesheke station were on the average in good physical agreement with PET on cool-dry days (64.3%) from DOY 74-191 and hot-dry days (29.4%) from DOY 197-292 (Figure 12). However, they were above PET on warm-wet days (104%) from DOY 325-74. This was attributed to change of surface conditions in the rain season during 'mixed' plant blooms. These surface conditions diverge from the assumed ones for the Penman-Montieth model. This highlighted the difficulties of evaluating AET using PET.

A comparison of SEBS station pixel and average grass fluxes with ECMWF estimates showed agreement on a few days, especially on cool-dry and hot-dry days. The SEBS

fluxes were largely greater than PET and ECMWF estimates between DOY 338 and 71, a period associated with high rainfall events and increased soil water. This period spans from December to March. As such there was high moisture content available for evapotranspiration. This period spans from December to March. Furthermore, the comparison with grass evaporative rates also indicated that the SEBS fluxes were physically consistent with PET on a number of days and in good agreement with ECMWF estimates for a few days (Figure 12).

The SEBS results were also evaluated in the northern parts of the study area at Kamanga station. This was done to check if the results would be similar to those observed at Sesheke station. The modelled evaporative fluxes at this station were compared with the ECMWF estimates only due to the lack of meteorological data needed to compute PET at satellite passing time. The comparison of modelled fluxes with ECMWF estimates on warm-wet days at Kamanga station is shown in Figure 13. Results indicated that the SEBS modelled fluxes were higher than ECMWF estimates on all the days except for DOY 336. On the average, SEBS fluxes were ~159% of ECMWF estimates. This implied that the modelled evaporative fluxes were not in good agreement with ECMWF estimates on many days around Kamanga station. This also indicated that the SEBS evaporative fluxes were higher in the northern parts of the semiarid Barotse basin than those in the southern parts, as observed at Sesheke station.

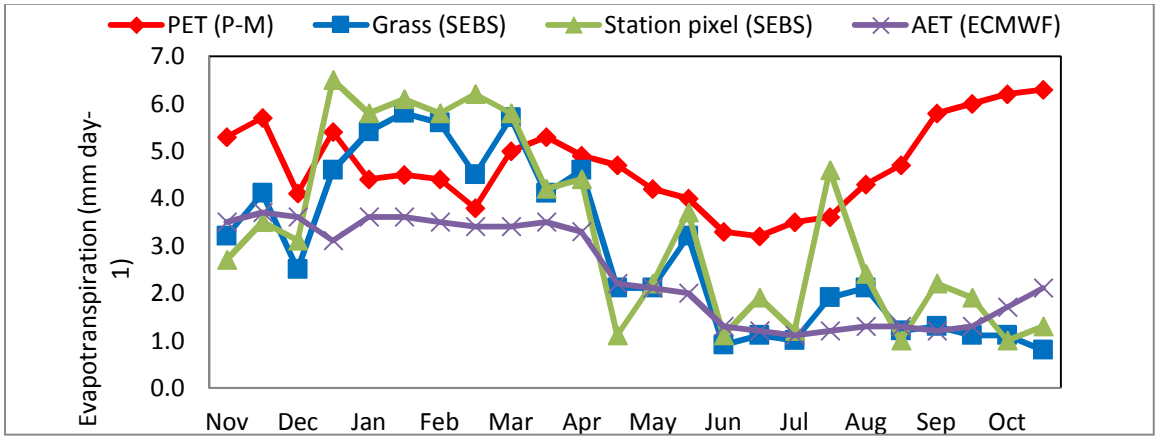

Figure 12: Comparison of SEBS AET with PET and ECMWF estimates at Sesheke station

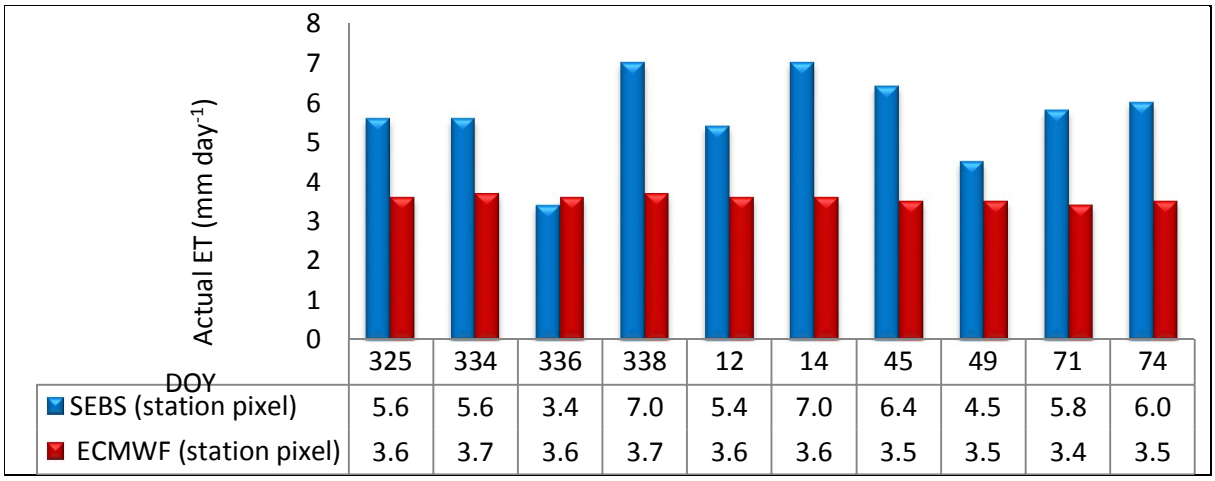


| DOY | 325 | 334 | 336 | 338 | 12 | 14 | 45 | 49 | 71 | 74 |
|---|---|---|---|---|---|---|---|---|---|---|
| SEBS (station pixel) | 5.6 | 5.6 | 3.4 | 7.0 | 5.4 | 7.0 | 6.4 | 4.5 | 5.8 | 6.0 |
| ECMWF (station pixel) | 3.6 | 3.7 | 3.6 | 3.7 | 3.6 | 3.6 | 3.5 | 3.5 | 3.4 | 3.5 |

Figure 13: Comparison of SEBS actual ET with ECMWF estimates on warm-wet days at Kamanga station

The differences between the SEBS fluxes and ECMWF estimates on cool-dry days at Kamanga station are shown in Figure 14. The SEBS fluxes were higher than ECMWF estimates on all cool-dry days except for one DOY 113. On the average, these fluxes were ~171% of ECMWF estimates. This means that the SEBS estimates at Kamanga station were much higher than those found at Sesheke station and not in good agreement with ECMWF estimates.

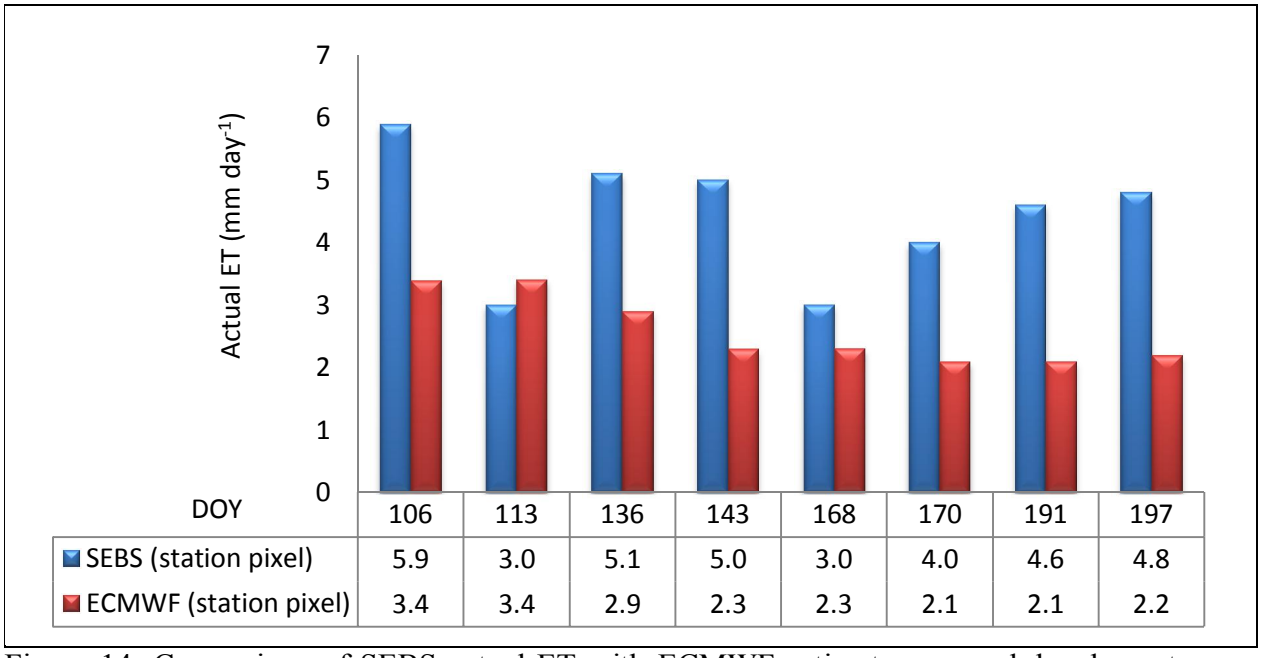


| DOY | 106 | 113 | 136 | 143 | 168 | 170 | 191 | 197 |
|---|---|---|---|---|---|---|---|---|
| SEBS (station pixel) | 5.9 | 3.0 | 5.1 | 5.0 | 3.0 | 4.0 | 4.6 | 4.8 |
| ECMWF (station pixel) | 3.4 | 3.4 | 2.9 | 2.3 | 2.3 | 2.1 | 2.1 | 2.2 |

Figure 14: Comparison of SEBS actual ET with ECMWF estimates on cool-dry days at Kamanga station

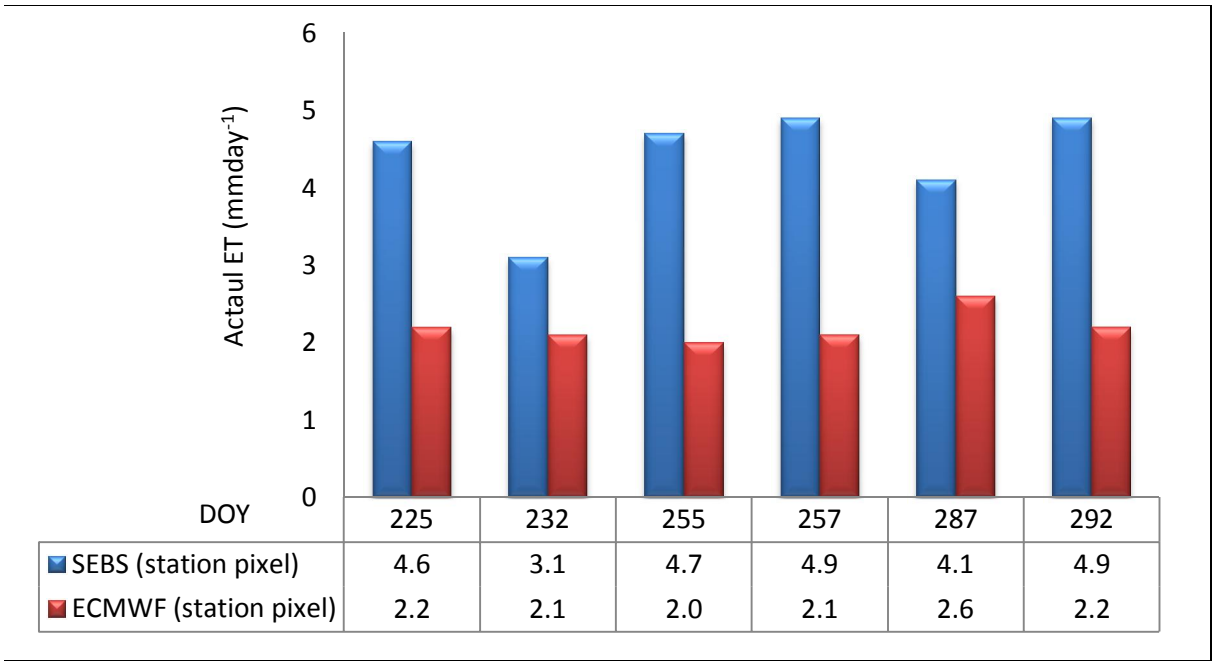


| DOY | 225 | 232 | 255 | 257 | 287 | 292 |
|---|---|---|---|---|---|---|
| SEBS (station pixel) | 4.6 | 3.1 | 4.7 | 4.9 | 4.1 | 4.9 |
| ECMWF (station pixel) | 2.2 | 2.1 | 2.0 | 2.1 | 2.6 | 2.2 |

Figure 15: Comparison of SEBS actual ET with ECMWF estimates on hot-dry days at Kamanga station

The comparison of the SEBS fluxes with ECMWF estimates on hot-dry days at Kamanga station indicated that the former were consistently higher than the latter (Figure 15). On the average, these fluxes were nearly twice (199%) those estimated by the ECMWF model. In comparison with the results observed at Sesheke station, the SEBS evaporative fluxes at Kamanga station were very high and not in good agreement with ECMWF estimates. The possible causes behind these discrepancies are discussed in section 5.

**The effect of aerodynamic roughness height for momentum transfer on ET estimates**

The fluxes per land cover type estimated using landuse-based and NDVI roughness values were compared on DOY 12 (Figure 16). It was observed that ET derived using landuse $Z_{om}$ was lower than that based on NDVI $Z_{om}$, especially over forests areas. Broadleaved deciduous forests (50) had a reduction of up to 25% which was equivalent to 1.5 mm day$^{-1}$. The lowest reduction occurred on water bodies (210).

**Evaluation of modelled SEBS evaporative fluxes at a monthly time scale**

The comparison of mean monthly AET with PET and rainfall estimates is shown in Figure 17. It is shown that monthly AET was largely lower than PET. However, it was higher than rainfall except from October to December. Monthly AET is expected to be lower than rainfall in given year in the absence of irrigation. In this study, however, the reference station is located in a heterogeneous area. It is near wetlands and water bodies and surrounded by closed to open shrublands. In the use of satellite data to calculate ET, the accuracy depends, in part, on the resolution of the sensor data (McCabe and Woods, 2006). In composite areas, there is lower confidence in variables obtained from low resolution sensor data because of the loss of intra-pixel spatial heterogeneity due to the integration of the radiometric signal (Gibson et al., 2011).

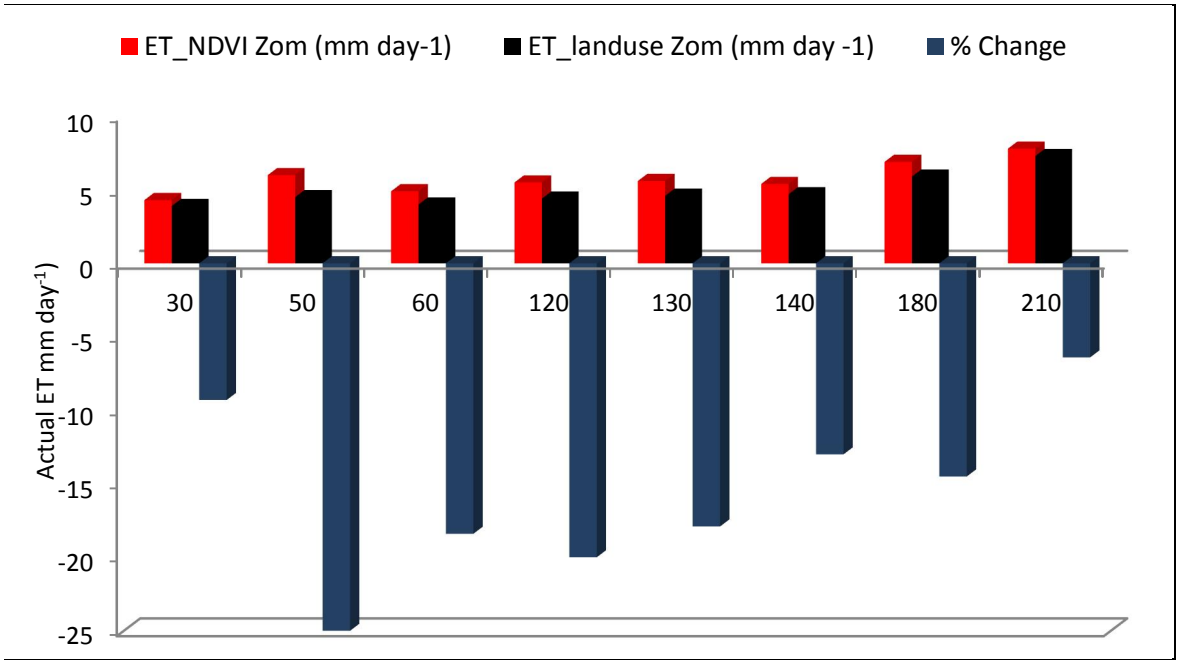

Figure 16: Effect of NDVI and landuse-based roughness on ET estimates on DOY 12 in the semiarid Barotse basin

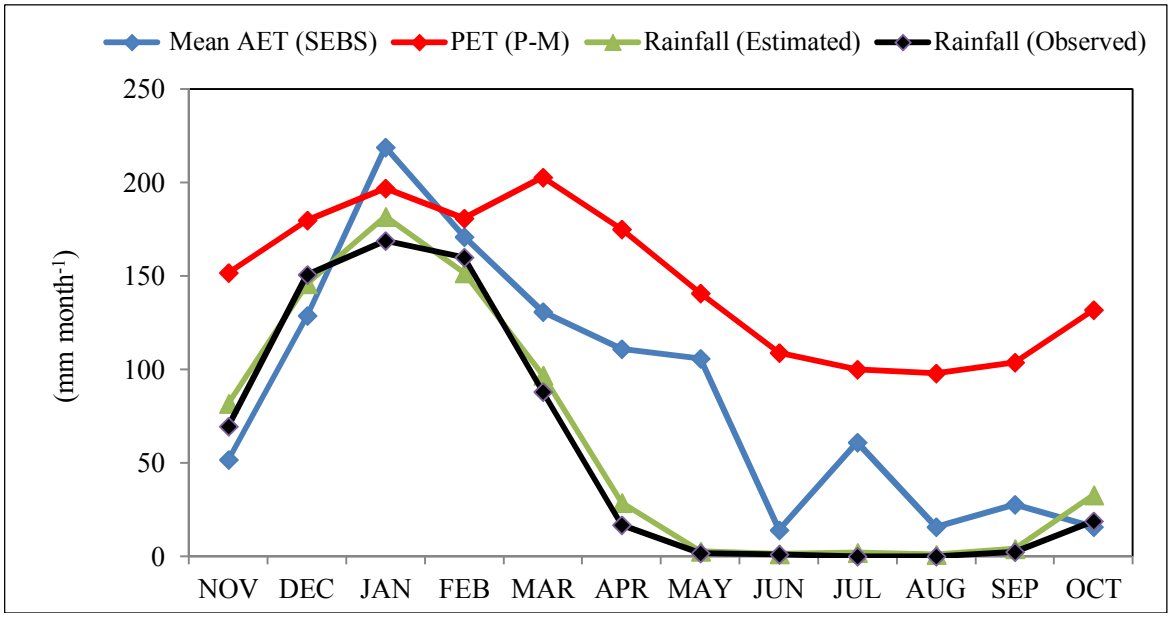


Figure 17: Comparison of modelled monthly AET with PET and rainfall at Sesheke station

The comparison of modelled monthly actual fluxes with ECMWF estimates and PET at Sesheke station is shown in Figure 18. Mean monthly actual fluxes were either above or below the ECMWF estimates.

The modelled monthly fluxes were higher than ECMWF estimates mainly in the warm-wet and cool-dry seasons. On the other hand, the fluxes were far below the ECMWF estimates in the dry season (August to October). This indicated that modelled fluxes were not in good agreement with ECMWF estimates.

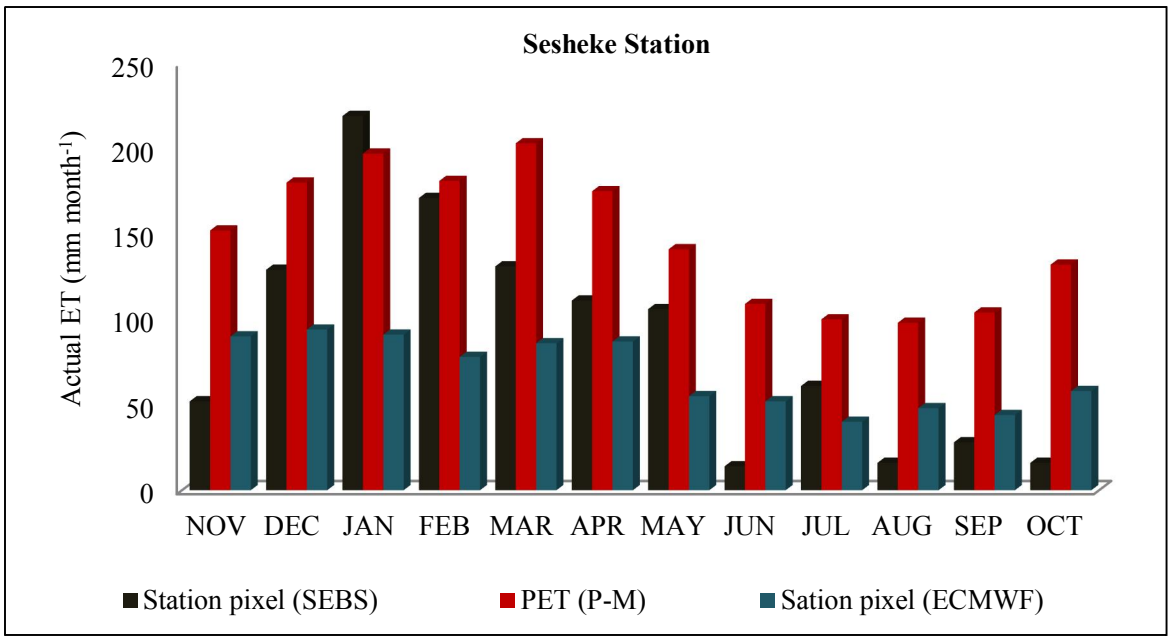


Figure 18: Comparison of SEBS monthly AET fluxes with PET and ECMWF estimates at Sesheke station

The modelled monthly evaporative fluxes were also compared with ECMWF estimates

at Kamanga station (Figure 19). It was observed that the modelled monthly fluxes were higher than ECMWF estimates in all the months except for June at this station. The SEBS fluxes were found to be very high in comparison with ECMWF estimates from November to January (Figure 19). The possible causes of lack of agreement between the modelled fluxes and ECMWF monthly estimates are also discussed in section 5.

## DISCUSSION

The modelled evaporative fluxes were in good physical agreement with PET on cool-dry and hot-dry days at Sesheke station. This was expected. The decline in soil moisture in the cool-dry season induces lower rates of ET whereas PET is not affected by this change. The depletion of soil moisture in the hot-dry season due to high atmospheric demand and deep percolation in the semi-arid Barotse basin reduces ET further whereas PET rises because of the increase in energy at the surface (cf. Vogt and Niemeyer, 2001; Suleiman and Richie, 2003). Thus, the physical agreement between SEBS and PET estimates shows that the former responded to the restrictions imposed by soil moisture on cool-dry and hot dry days.

The lack of physical agreement between SEBS and PET estimates on warm-wet days was attributed to the effect of change in surface conditions. The Penman-Montieth model assumes that the ground is completely covered by short grass, the so called 'big leaf'. However, plant species co-exist very often and there is a period when the vegetation is not 'closed' (Shuttleworth and Wallace, 1985). This means that both the soil surface and vegetation leaves evaporate moisture and their importance change as plant species develop. This may have caused the modelled fluxes to be higher than PET (cf. Hailegorgis, 2006).

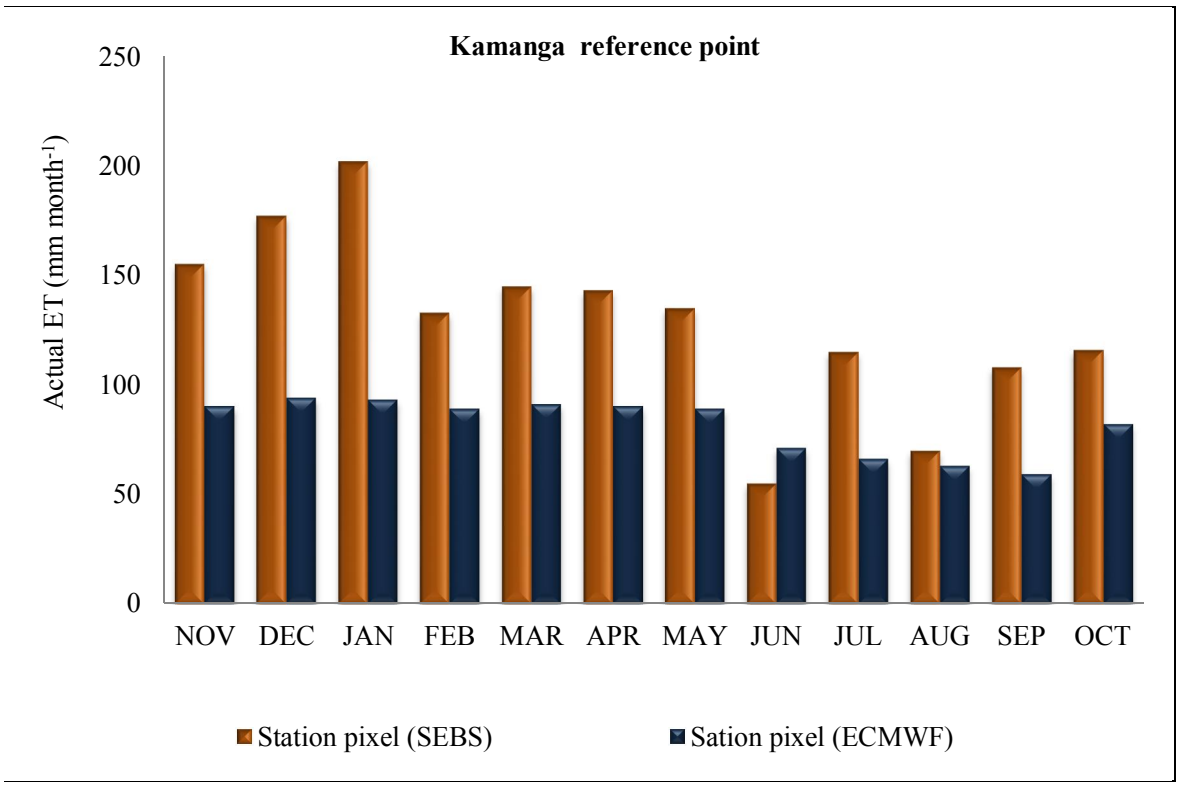


Figure 19: Comparison of SEBS fluxes with PET and ECMWF estimates at Kamanga reference station

Thus systematic occurrence of physically inconsistent fluxes on warm- days rather suggested that surface conditions were different from those assumed for PET model. This highlights the uncertainties of evaluating actual evaporative fluxes against PET in heterogeneous environments.

The SEBS evaporative rates differed from ECMWF estimates in that the former were mainly higher than the latter. However, it was observed that these fluxes were in better agreement with ECMWF estimates at Sesheke station on a number of days than at Kamanga. The lack of good agreement between the evaporative fluxes modelled by the SEBS and ECMWF were ascribed to a number of factors.

On the one hand, the lack of good agreement between SEBS and ECMWF estimates could have come about because of differences in the parametrisation of turbulent heat fluxes. In addition to this, the SEBS model used in this study was run using the 1Km resolution of MODIS imagery whereas the ECMWF model has a course resolution of ~50 kilometres at best. Given that surface conditions can be highly variable in space and time, especially for heterogeneous areas, the course resolution of ECMWF model may be questioned if it can adequately capture these variations in the semi-arid Barotse basin (cf. Vogt and Niemeyer, 2001). This means that the resulting evaporative fluxes from the ECMWF model may not be as highly variable as the surface conditions because of its course resolution. For future studies, therefore, it is proposed that a statistical downscaling method should be employed to find the relationship between actual AET in the study area and ECMWF estimates.

On the other hand, modelled fluxes were higher than ECMWF estimates due to uncertainties associated with surface parameterisation. In this study, a vegetation index (NDVI) was used to model surface roughness, canopy height, displacement height, fractional vegetation cover and the ground heat flux. It is observed that estimating roughness height for momentum transfer from NDVI is problematic over high vegetation areas such as forests as the value tends to be too small (Rauwerda et al., 2002; Su, 2005). Conversely, the value tends to be overestimated over short but very green plant species (Hailegorgis, 2006). In this study, the estimated roughness values were lower over forested areas and slightly higher over grassland and cropland compared to reported literature values (eg Wieringa, 1993; Mücher et al. 2001; Su, 2005; Alvarez 2007). Thus, NDVI-based values used in this study affected the accuracy of the results, as shown in Figure 16 (c.f. Hailegorgis, 2006; Lin, 2006; Alvarez, 2007; van der Kwast et al., 2009; Gebreyesus, 2009). This means that estimating roughness using more robust methods can improve the results of the modelled fluxes. The challenge, however, is that the alternatives such as LIDAR data or detailed roughness maps are often not available.

The use of the fraction vegetation cover, which was derived from NDVI using the method of Sobrino et al. (2003), is also likely to have caused higher flux estimates. In this study, fraction vegetation cover was used to calculate the excessive resistance term ($kB^{-1}$), emissivity ($\varepsilon$) and parameterize ground heat flux ($G_o$). It is known that using this method underestimates the latter value due to solar zenith and azimuth angle in addition to the orientation of the tree rows which allowed bare soil underneath the tress to receive direct radiation (Gibson et al., 2011). Consequently more energy is left to be shared between sensible and latent heat fluxes. Calibrating the fraction vegetation cover by deriving scene-specific NDVI maximum and minimum, as suggested by Gibson et al. (2011), is likely to improve the flux estimates.

With regard to uncertainties associated with meteorological input data, the use of average near surface temperature may have

contributed to higher flux estimates, especially in the northern parts of the study area. This area is not covered by a functional meteorological station. Thus, average temperature was used as interpolated surfaces could not be built. It has been shown, however, that the SEBS model is very sensitive to, among other parameters, the input data of air temperature (Badola, 2009) or land surface and air temperature gradient (Gibson et al., 2011). Thus, the accuracy of the estimates in the study area is also likely to improve if distributed temperature, which is validated on a number of ground stations, is used.

## CONCLUSION

This study was aimed at estimating the spatio-temporal variability of AET in the semiarid Barotse basin on clear-sky warm-wet, cool-dry and hot-days using the SEBS model, and upscaling these to monthly fluxes using sunshine data. Evaluation of the modelled results was done using PET and ECMWF estimates. Despite all the challenges in obtaining suitable reference data, the SEBS model has been shown in this study to realistically estimate spatio-temporal variability of actual fluxes over heterogeneous areas. The SEBS fluxes evaluated against PET at Sesheke station showed that they were in physical agreement and the lack of it on warm-wet days did not mean that the estimates were implausible. This is because the model estimates AET from the actual ground as compared to the Penman-Montieth equation, which uses a reference surface. There were indications, however, that model outputs could have been overestimated when compared with ECMWF and rainfall estimates. Fortunately, the causes of lack of agreement with these estimates could be related to known problems such as lack of spatial input data and reliance of NDVI to parameterise roughness. With respect to the latter, it was demonstrated that use of one of alternative ways, landuse-based aerodynamic roughness, can counter part of the problem of overestimating of fluxes, especially over forests. Further research on how to estimate this parameter along with finding distributed meteorological data, should improve the accuracy of the model in such catchments. Thus, with accurate surface parametrisation and meteorological data, remote sensing and the SEBS model can be successfully used to quantify spatio-temporal evaporative fluxes over heterogeneous areas and contribute towards water resources management. The challenge in achieving the required accuracy, however, lies in obtaining spatial input data at catchment and basin level. This means that once reliable sources of such data are found, model results would also improve and decision makers in government, private sector and civil society can use this to quantify water resources and determine water use at a catchment level.

## ACKNOWLEDGEMENTS

This work was carried out with the financial and technical support of and within the framework of Tiger Africa Capacity Building Initiative for the application of satellite remote sensing to support water resources management in Africa under project Number 026 allocated to Zambia under Integrated Water Resources Management Centre of the University of Zambia (UNZA-IWRM). The first author would like to thank the Danish International Development Agency (DANIDA), Royal Danish Embassy in Lusaka and Ministry of Energy and Water Development (MEWD) for the generous financial resources used for the fieldwork campaign.

## REFERENCES

Allen, R.G., Pereira, L.S., Raes, D., Smith, M., 1998. Crop evapotranspiration. Guidelines for computing crop water requirements-FAO Irrigation and Drainage Paper No. 56 FAO, Rome, Italy.

Alvarez, J.A.G., 2007. Effects of land cover changes on the water balance of Palo Verde

Wetland, Cost Rica, M.Sc. Thesis, ITC, The Netherland, pp. 13-72.

Badola, A., 2009. Validation of Surface Energy Balance System (SEBS) over forest land cover and sensitivity analysis of the model, MSc thesis, International Institute for Geo-information Science and Earth Observation, The Netherlands, p. 59.

Bicheron, P., Brockmann, C., Schuten., L., Vancutsen, C., Huc, M., Boutemp, S., Leroy, M., Achard, F., Herold, M., Ranera, F., Arino, O., 2008. The ESA-Globcover Project, MEDIAS-France.

Brutsaert, W., 1982. Evaporation into the atmosphere: Theory, History, and applications, Reidal Publishing, New York, p. 299.

Carlson, T.N., Capehart, W. J., and Gillies, R.R., 1995. A new look at the simplified method for remote-Sensing of daily evapotranspiration. Remote Sensing of Environment, 54, 61-67.

Choudhury, B.J., Ahmed, N. U., Idso, S.B., Reginato, R.J., and Daughtry, C.S.T., 1994. Relations between evaporation coefficients and vegetation indices studied by model simulations, Remote Sensing of Environment, 50 (1): 1-17.

Courault, D., Seguin, B., Olioso, A., 2005. Review on estimation of evapotranspiration from remote sensing data: From empirical to numerical modelling approaches. Irrigation and Drainage Systems, 19: 223–249.

Desanker, P.V., Frost, P.G.H., Frost, C. O., Justice, C.O., Scholes, R.J., 1997. The Miombo Network: Framework for a terrestrial transect study of land-use and land-cover change in the miombo ecosystems of Central Africa, The International Geosphere-Biosphere Program (IGBP), Report 41, Stockholm, p. 74.

Flint, L., 2006. Climate change, vulnerability and the potential for adaptation: case-study – the Upper Zambezi Valley region of Western Zambia, University of Copenhagen, Denmark, p. 17.

Food and Agriculture Organisation (FAO) and Government of Republic of Zambia (GRZ), 1986. Soil map of Zambia, www.eusoils.jrc.eceuropa.eu/esdb_archive/ EUDASM/Africa/lists/si_czm_html.

Gebreyesus, M. G., 2009. Validation of RS approaches to model surface characteristics in hydrology: a case study in Guarena Aquifer, Salamanca, Spain, MSc thesis, International Institute for Geo-information Science and Earth Observation, The Netherland, p. 65

Gibson, L.A., Münch, Z., and Engelbrecht, J., 2011. Particular uncertainties encountered in using a pre-packaged SEBS model to derive evapotranspiration in a heterogeneous study area in South Africa. Hydrol. Earth Syst. Sci. 15 (1), 295–310.

Gokmen, M., Vekerdy, Z., Verhoef, A., Verhoef, W., Batelaan, O., and van der Tol, C., 2012. Integration of soil moisture in SEBS for improving evapotranspiration estimation under water stress conditions, In: Remote sensing of environment,121(2012) pp. 261-274.

Hailegiorgis, W.S., 2006. Remote sensing analysis of summer time evapotranspiration using SEBS algorithm: A case study of Regge and Dinkel, The Netherlands, M.SC. Thesis submitted to the International Institute for Geo-information Science and Earth Observation, pp. 42-88.

Hagreaves, G.H and Samani, Z.A., 1985. Reference crop evapotranspiration from temperature. Appl. Eng. Agric., 1 (2): 96-99.

Huxman, T., Wilcox, B., Breshears, D., Scott, R., Snyder, K., Small, E., Hultine, K., Pockman, W., Jackson, R., 2005. Ecohydrological implications of woody

plant encroachment Ecology, 86: 308–319.

Irmak, S., 2009. Estimating crop evapotranspiration from reference evapotranspiration and crop coefficients**,** University of Nebraska-Lincoln Extension Neb Guide G1994, p. 4.

Jackson, R.D., Reginato, R.J., and Idso, S.B., (1977), Wheat canopy temperature: A practical tool for evaluating water requirements. Water Resource Research 13: 651–656.

Jia, L., Su, Z., Van den Hulk, B., Menenti, M., Moene, A., De Bruin, H.A.R., Yrisarry, J.J.B., Ibenez, M., Cuesta, A., 2003. Estimation of sensible heat flux using the Surface Energy Balance System (SEBS) and ATSR measurement, physics and Chemistry of the Earth, 28 (1-3): 75-88.

Jia, L., Xi, G., Liu, S., Huang, C., Yan, Y., Liu, G., 2009. Regional estimation of daily to annual regional evapotranspiration with MODIS data in the Yellow River Delta wetland. Hydrol. Earth Syst. Sci. 13 (10): 1775–1787.

Khan, S.I., Hong, Y., Vieux, B., and Liu, W., 2010. Development and evaluation of actual evapotranspiration estimation algorithm using satellite remote sensing and meteorological observation network in Oklahoma in: International Journal of Remote Sensing, Vol. 31, No. 14, 20 July, 3799-3819, online ©Taylor and Francis,@ www.tandf.co.uk/journal.

Kustas, W.P., and Daughtry, C.S.T., 1990. Estimation of soil heat flux/net radiation ratio from spectral data. *Agric.* Forest. Meteorol., 49: 205-223.

Liang, S., 2001. Narrowband to broadband conversions of land surface albedo I: Algorithms. Remote Sensing of Environment 76 (2): 213-238.

Lin, W., 2006. Satellite based regional scale evapotranspiration in the Hebei Plain, Northeastern China, M.Sc. thesis, International Institute for Geo-information Science and Earth Observation, The Netherlands, p. 66.

McCabe, M.F., and Wood, E.F., 2006. Scale influence on the remote estimation of evapotranspiration using multiple satellite sensors, Remote Sens. Environ., 105: 271-285.

MacClatchey, R. A., and Selby, J. E., 1972. Atmospheric transmittance from 0.25 to 38.5 mm: computer code LOWTRAN-2, Air Force Cambridge Research Laboratories, AFCRL-72 0745, Environ. Res. Paper 427.

Monin, A. S., and Obukhov, A.M., 1945. Basic laws of turbulent mixing in the surface layer of the atmosphere, Tr.Akad. Nauk SSSR Geophiz. Inst., 24(151), 163-187.

Moran, M.S., 2004. Thermal infrared measurements as an indicator of plant ecosystem health, in: Thermal remote sensing in land surface processes, edited by: Quattrochi, D. A., and Luvall, J.,Taylor and Francis, CRC Press, Boca Raton, USA, 257–282.

Monteith, J.L., and Unsworth, M.H., 1990. Principles of environmental physics, Edward Arnold, London.

Mücher, C.A., Steinnocher, K., Champeaux, J.L., Griguolo, S., Wester, K. Loudjani, P., 2001. Land cover characterization for environmental monitoring of Pan-Europe, Wageningen University and Research Centre, Centre for Geoinformation: http://cgi.girs.wageningenur. nl/cgi/projects/eu/pelcom/public/index.htm.

Penman, H. L., 1948. Natural evaporation form open water, bare soil, and grass.Proc. Roy. Soc., 193: 120-146.

Priestley, C.H.B., and Taylor, R.J., 1972. On the assessment of surface heat flux and

evaporation using large-scale parameters. Month. Weather Rev. 100 (2): 81–92.

Rahman, H., and Dedieu, G., 1994. SMAC: a simplified method for the atmospheric correction of satellite measurements in the solar spectrum. International Journal of Remote Sensing, 15(1): 123-143.

Rauwerda, J., Roerink, G.J., Su, Z., 2002. Estimation of evaporative fractions by the use of vegetation and soil component temperatures determined by means of dual-looking remote sensing, Alterra,Green World Research, Wageningen, pp. 12-47.

Rwasoka, D.T., Gumindoya, W., Gwenzi, J., 2011. Estimation of actual evapotranspiration using the surface energy balance system (SEBS) algorithm in the Upper Manyame Catchment in Zimbabwe, J. Phys.Chem. Earth, doi:10.1016/j.pce.2011.07.035.

Seguin B., and Ittier B., 1983. Using midday surface temperature to estimate daily evaporation from satellite thermal IR data, International Journal of Remote Sensing Environment, 4: 371–383.

Shan, X., van de Velde, R., Wen, J., He, Y., and Su, Z., 2007. Regional evapotranspiration over the Arid Inland Heihe River Basin in Northwest China, ESA's Publications Division as Special Publication SP-655, Proceedings of the Dragon Programme final results.

Shuttleworth, W.J., and Wallace, J.S., 1985. Evaporation from sparse crops-An energy combination theory, Quaterly Journal of the Royal Meteorology Society, 11: 893-855.

Suleiman, A.A., and Richie, J.T., 2003. Modelling soil water redistribution under second stage evaporation, Soil Sci.Soc. Am. J., 67 (2): 377-386.

Sobrino, J.A., Kharraz, J.E., Li, Z., 2003. Surface temperature and water vapour retrieval from MODIS data. International Journal of Remote Sensing, 24 (24), 5161–5182.

Su, Z., 2002. The Surface Energy Balance System (SEBS) for estimation of turbulent heat fluxes. Hydrology and Earth System Sciences, 85-99.

Su, Z., Schmugge, T., Kustas, W.P., and Massman, W.J., 2001. An evaluation of two models for estimation of the roughness height for heat transfer between the land surface and the atmosphere, Journal of Applied Meteorology, 40 (11): 1933-1951.

Su, Z., and Jacobs, C., 2001. Advanced earth observation: Land surface climate final report, Delft: Beleidscmmissie Remote Sensing (BCRS), UPS report, p. 57.

Su, Z., Yacob, A., He,Y., Boogaard, H., Wen, J., Gao, B., Roerink, G., van Diepen, K., 2003. Assessingrelative soil moisture with remote sensing data: theory, experimental validation, and application to drought monitoring over the North China Plain, Physics and Chemistry of the Earth, 28 (1-3): 89-101.

Su, Z., 2005. Estimation of the surface energy balance. In: Encyclopedia of hydrological sciences: 5 Volumes. / ed. by Anderson, M.G., McDonnell , and Chichester , J.J., Wiley and Sons, ISBN: 0-471-49103-9. Vol. 2 pp. 731-752.

Tucker, C. J., 1979. Red and photographic infrared linear combinati ons for monitoring vegetation, Remote Sensing of Environment 8:127-150.

van der Kwast, J., Timmermans, W., Gieske, A., Su, Z., Olioso, A., Jia, L., Elbers, J., Karssenberg, D., de Jong, S., 2009. Evaluation of the Surface Energy Balance System (SEBS) applied to ASTER imagery with flux-measurements at the SPARC 2004 site (Barrax, Spain), Hydrol. Earth Syst. Sci. 13 (7): 1337–1347.

Vogt, J., and Niemeyer, S., 2001. Integration of operationally available remote sensing and synoptic data for surface energy balance modelling and environmental applications on the regional scale in: Beniston, M., and Verstraete, M.M., (eds.), (2003), Remote sensing and climate modelling synergies and limitations, Kluwer Academic Publishers, New York, USA, pp. 329-343.

Wieringa, J., 1993. Representative roughness parameters for homogenous terrain, In: Boundary Layer Meteorology, 63(1993), pp. 323-363.